NANO LETTERS

pubs.acs.org/NanoLett
Letter

Cu Nanoparticle Infiltration via Metal–Organic Decomposition Ink for Superior Mass Activity in CO Electroreduction

Juhyung Choi,[#] Sejin Park,[#] Dayeon Kim, Hyun Chul Kim, Hyewon Yun, Yewon Hong, Hyun Ji An, Taemin Lee, Noho Lee, Jaeeun Kim, Dae-Hyun Nam, Hyung-Suk Oh, and Yun Jeong Hwang*

Cite This: *Nano Lett.* 2025, 25, 15346–15352

ABSTRACT: Achieving stable operation at high currents remains challenging for gas diffusion electrode (GDE)-based CO electrolyzers. Herein, we demonstrate the importance of Cu nanoparticle infiltration into the microporous layer to enrich local CO accessibility and mitigate electrolyte crossover. A facile GDE preparation method is developed via the doctor-blading method using a Cu metal–organic decomposition (Cu MOD) ink to produce well-dispersed nanoparticles across the porous layer. This design produces highly selective C_{2+} products at −1200 mA cm^{-2} from the CO electroreduction reaction, achieving a remarkably high mass activity of approximately −28,000 A g^{-1}. It is found that the Cu electrodes prepared by MOD improve a stable balanced gas–liquid–solid interface by CO transport across the hydrophobic microenvironment of the inherent microporous layer. Our insights offer perspectives on a scalable strategy for optimizing catalyst positioning and advancing stable GDEs with high mass activity.

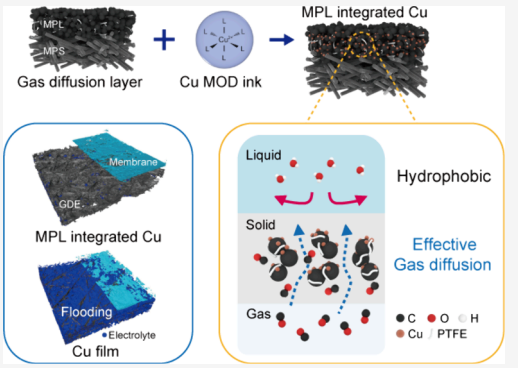

KEYWORDS: *Cu metal–organic decomposition ink, Microporous layer, Hydrophobicity, CORR*

Electrochemical $CO_{(2)}$ reduction reactions ($CO_{(2)}$RRs) have been investigated for the sustainable production of chemical feedstocks and fuels.[1−3] The conversion of CO_2 to C_{2+} products is proposed, but local pH increases pose challenges in achieving high performance due to changes in product selectivity, loss of CO_2 to carbonate, and salt formation. Unlike the CO_2RR, the CORR can operate under alkaline conditions without carbon loss and can generate C_{2+} products with high selectivity, and provide fundamental insights.[2−5]

The gas diffusion electrode (GDE)-based electrolyzers become crucial to facilitate CO transport across the gas diffusion layer (GDL) and position the catalyst layer near the gas–liquid interface because of the low solubility of CO (approximately 1 mM).[6−8] However, when obtaining high current densities, the hydrogen evolution reaction (HER) becomes rather more pronounced. High potentials and catalyst reconstruction cause electrowetting, which causes flooding of the electrode and reduces catalytic selectivity.[9−11] To prevent water penetration, surface modification to increase the hydrophobicity of the surface has been used, for example, by introducing polytetrafluoroethylene (PTFE) and other materials.[12−14] Despite these efforts, the surface wettability of the cathode still changes rapidly by $CO_{(2)}$RR.[15,16] Another challenge relates to the gas diffusion to the catalyst surface,[15,17,18] when catalyst particles are loaded onto porous GDLs. The particle size or its dispersion blocks the porosity and gas permeability across the GDE, reducing the effective surface area.

Consequently, catalyst preparation strategies that incorporate catalyst particles across a porous GDL should be developed to balance gas transport and surface wettability. Cu metal–organic decomposition (MOD) inks have been widely utilized to fabricate electrical metal contacts on various substrates to achieve uniform coating on rough surfaces with strong adhesion,[19−21] promising for uniform deposition in porous structures. Cu MOD inks comprise a metal precursor and complexing reagents and can be printed onto a wide range of substrates, enabling submicrometer-scale patterning. Subsequently, the organic ligands are calcinated in a reductive atmosphere, even at low temperatures (*ca.* 200 °C), yielding elemental Cu.[20] This low-temperature process is advantageous for Cu electrocatalyst adhesion on porous electrodes, and additional binders are not required. Moreover, the adjustable viscosity of the ink allows it to penetrate the porous GDL electrode.

Received: August 7, 2025
Revised: October 1, 2025
Accepted: October 3, 2025
Published: October 12, 2025

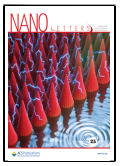

https://doi.org/10.1021/acs.nanolett.5c04051
Nano Lett. 2025, 25, 15346−15352

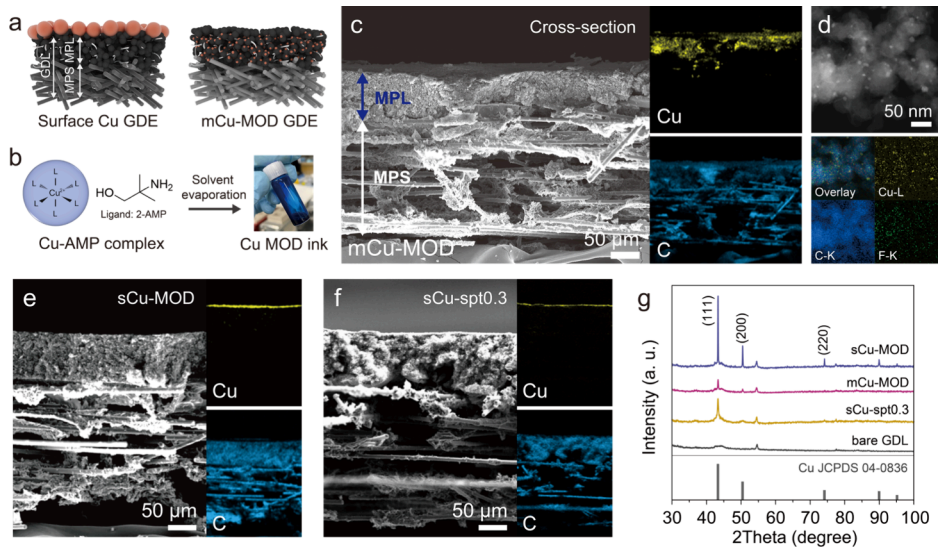

Figure 1. (a) Schematic of sCu-MOD GDE (left) and mCu-MOD GDEs (right) and (b) Cu MOD ink through the Cu-AMP complex. Low-magnification cross-sectional SEM and the corresponding EDS mapping images of (c) mCu-MOD, (e) sCu-MOD, and (f) sCu-spt0.3, respectively. (d) S-TEM image and the corresponding EDS mapping image and spectrum of the microporous layer in mCu-MOD. (g) X-ray diffraction patterns of bare GDL, sCu-spt0.3, sCu-MOD, and mCu-MOD.

Here, we develop to incorporate metallic Cu nanoparticles (NPs) into the microporous layer (MPL) of a GDL using MOD ink without any additives, which allows Cu to exploit the inherently porous and hydrophobic properties of the MPL. The CORR performance shows superior mass activity (−27,896 A g^{-1}) and C_{2+} selectivity (Faradaic efficiency (FE) 86.6%) in an alkaline flow cell. Notably, it was found that flooding at high current densities is suppressed by Cu MOD preparation owing to surface hydrophobicity and efficient gas transport, attributed to the well-dispersed Cu NPs over the MPL. The Cu MOD electrode configuration demonstrated a higher activity by modulating the microenvironment, monitored by water fraction under electrocatalytic reactions. This study provides a useful electrode fabrication strategy for incorporating catalysts into MPL based on a Cu MOD ink that is also applicable to other metals for enhanced, stable electrocatalysis.

Our strategy is to decompose the Cu precursors directly within the MPL, yielding a uniform NP layer coating and providing two key advantages: (1) increased hydrophobicity in the local microenvironment of the active catalyst and (2) efficient CO gas transport at the Cu catalyst−electrolyte interfaces. Uniform Cu metal deposition within the MPL was achieved by utilizing a Cu-MOD ink (Figures 1a and 1b), denoted mCu-MOD. The precursor solution comprised Cu(II) formate and 2-amino-2-methyl-1-propanol (2-AMP) complex (Cu-AMP complex) in methanol. After evaporating the solvent, the Cu-MOD ink seamlessly diffused into the approximately 80 μm-thick MPL and was adjusted by a blade-printing process (Figure S1a). Then, the Cu(II) was thermally reduced to metallic Cu in Ar, whereas the alkanolamine ligands of Cu-AMP complexes were completely oxidized.[20,22] The Cu-MOD ink is, thus, pyrolyzed to Cu NPs at a lower temperature (200 °C) than the melting point (327 °C) of the PTFE layer. The low temperature allows the deposition of Cu NPs into the PTFE while retaining its hydrophobic properties and porosity.

Cross-sectional scanning electron microscopy (SEM) images revealed that the GDL of carbon paper (Sigracet 39BB) substrate was well preserved with mCu-MOD after pyrolysis, and energy-dispersive X-ray spectroscopy (EDS) mapping confirmed a uniform Cu NP deposition (Figures 1c and S4a) down to the underside of the thick MPL, allowing deep Cu penetration. The SEM images of bare carbon paper confirm that the same GDL consists of an MPL and microporous substrate (MPS) having a thickness of ca. 300 μm (Figures S2 and S3). Transmission electron microscopy (TEM) images showed similarity to the bare MPL after mCu-MOD deposition (Figures S4b and S4c), and nanosized Cu particles were observed by scanning TEM (STEM) and EDS mapping (Figure 1d). MPLs were collected from the bare GDL and mCu-MOD-coated GDL to measure Brunauer−Emmett−Teller (BET) analysis. It reveals comparable porosity and specific surface areas of 32.75 and 31.24 m^2 g^{-1}, respectively (Figure S5), implying the porosity was not markedly affected by the deposition of mCu-MOD. However, the double-layer capacitance (C_{dl}) (Figure S6) of mCu-MOD (0.86 mF cm^{-2}) increased by over 100 times compared to that of the carbon paper (8.22×10^{-3} mF cm^{-2}), indicating their different electrochemical properties.

To investigate the effect of Cu infiltration, instead of the blade-printing method, Cu-MOD ink was spray-coated onto the MPL and annealed (denoted sCu-MOD) (Figure S1b). In contrast to the mCu-MOD, the sCu-MOD had a 3 μm-thick Cu surface coating on top of the MPL according to the cross-sectional SEM-EDS images (Figure 1e). Top-view images of sCu-MOD confirmed the densely packed Cu film (Figure S7). It indicates that the pressure applied by the blade printing method significantly improves the morphological infiltration of the Cu-MOD ink. We also prepared additional control surface Cu films by sputtering to 0.3 μm thickness (denoted sCu-spt0.3) (Figures 1f and S8). The X-ray diffraction (XRD) patterns of all three as-prepared electrodes matched well with the cubic phase of metallic Cu (JCPDS 04−0836) (Figure 1g).

To investigate how the method for loading Cu NPs affected the hydrophobicity of the electrode, we first measured the contact angle (CA). The CAs of bare carbon paper, mCu-MOD, and sCu-MOD were 138.3°, 133.9°, and 120.6°, respectively (Figure 2a), indicating that the hydrophobicity of

https://doi.org/10.1021/acs.nanolett.5c04051
Nano Lett. 2025, 25, 15346−15352

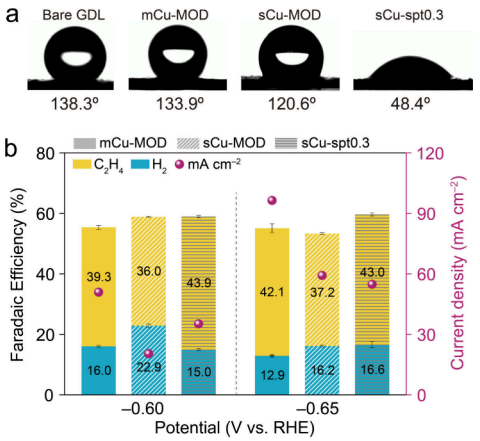

Figure 2. (a) CAs of bare GDL, mCu-MOD, sCu-MOD, and sCu-spt0.3 GDEs, respectively. (b) Product distributions and total current densities of the as-prepared Cu GDEs at various applied potentials (−0.60 and −0.65 V vs RHE) in CO-saturated 1.0 M KOH electrolyte measured in the H-cell system.

the GDE was well-preserved after Cu deposition using the MOD ink. In contrast, the Cu film sputtered on carbon paper (sCu-spt0.3) showed a noticeably decreased CA (48.4°) and became hydrophilic as the Cu thin film completely covered the MPL. The hydrophilicity of the GDE surface responded sensitively when the Cu film was completely covered. In particular, the blade-printing method (mCu-MOD) maintained a higher CA than the simple spraying method (sCu-MOD), indicative of efficient Cu infiltration into the MPL.

Next, we performed the CORR of the Cu GDEs using an H-cell (Figures 2b and S9) to estimate the catalytic activity. In the H-cell, the backside of the GDE was masked to confine the mass transport of dissolved $CO_{(aq)}$ and water to the front side of the MPL surface and not in other directions.[23] In the H-cell, while the dispersity of Cu NPs within the MPL layer is predicted to be less impacted, the catalytic activities of the exposed Cu surfaces can be evaluated. When the CORR activities were compared in 1.0 M KOH (Figures S9a–c), all Cu GDEs confirmed to have no significant differences in FEs for C_2H_4 and H_2, at −0.60 and −0.65 V_{RHE}. The FE for C_2H_4 of mCu-MOD (42.1%) was slightly higher than that of sCu-MOD (37.2%) at −0.65 V_{RHE}, and the mCu-MOD also achieved a higher current density (−96.4 mA cm^{-2}) than sCu-MOD (−59.2 mA cm^{-2}). Compared to the sputtered Cu, the maximum partial current density of the CORR was also larger in mCu-MOD and sCu-MOD, owing to the efficient infiltration of Cu NP by the MOD ink.[24] Furthermore, the more hydrophilic sCu-spt0.3 reduced the overpotential for the HER;[25] indeed, the HER became more pronounced when a thicker (1.2 μm) sputtered Cu film, denoted as sCu-spt1.2, was used. The CA of sCu-spt1.2 notably decreased to 27.4°, close to superhydrophilicity (Figures S9d and S10).

We investigated the effect of the surface hydrophobicity at a gas–liquid–solid boundary further, by comparing the CORRs in the flow cell (Figure 3a). At a current density of −400 mA cm^{-2}, the more hydrophilic sCu-spt0.3 showed high HER activity. In contrast, the GDEs prepared from Cu MOD ink achieved C_{2+} FEs of 87.8% and 82.4%, respectively. Whereas the sputtered Cu film on the carbon paper were readily flooded above −400 mA cm^{-2}, the Cu MOD surface effectively suppresses the HER and prevents electrolyte penetration into the porous layer under high current operation in a flow cell.[12,26] The Cu loadings were obtained by inductively coupled plasma–optical emission spectroscopy (ICP-OES) measurements, revealing that mCu-MOD has substantially lower Cu loading (0.043 mg cm^{-2}) than that of sCu-MOD (0.396 mg cm^{-2}) and sCu-spt0.3 (0.223 mg cm^{-2}) (Table S1). The mass activity of mCu-MOD for −27,896 A g^{-1} is about 11 times higher than that of sCu-MOD (−2,525 A g^{-1}). The high mass activity of mCu-MOD is among the best reported for Cu-based catalysts (Table S2), demonstrating the key role of Cu deposition. It is found that the uniform and small nanoparticle deposition of mCu-MOD plays a critical role in achieving a remarkably enhanced mass activity at −1200 mA cm^{-2}.

Additionally, to enable real-time water crossover depending on the morphology of Cu, we designed a customized electrolyzer with a window that allowed the direct observation

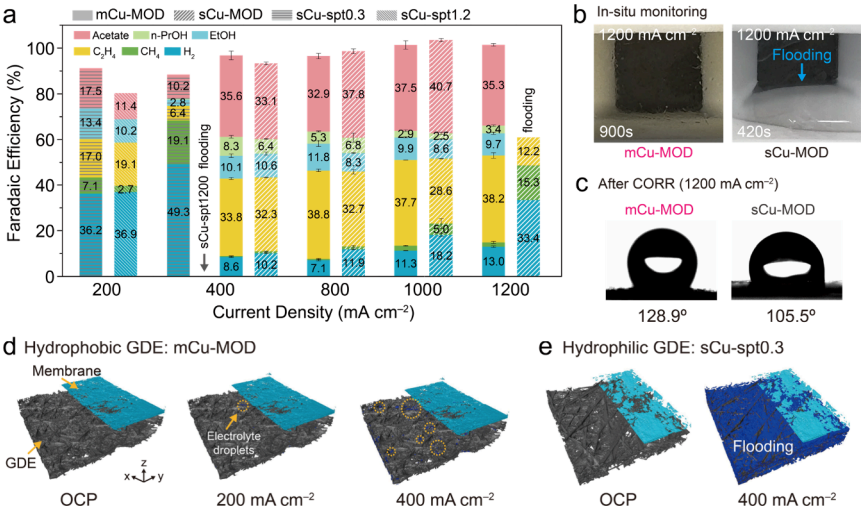

Figure 3. (a) Product distributions of CORR on mCu-MOD, sCu-MOD, sCu-spt0.3, and sCu-spt1.2 GDEs in the flow-cell system in the range from −200 to −1200 mA cm^{-2} in 1.0 M KOH. (b) In situ monitoring of the gas-diffusion region for mCu-MOD and sCu-MOD at a current density of −1200 mA cm^{-2}. (c) Change in the CA of mCu-MOD and sCu-MOD GDEs after CORR. In situ micro-CT 3D structure images of (d) mCu-MOD and (e) sCu-spt0.3.

https://doi.org/10.1021/acs.nanolett.5c04051
Nano Lett. 2025, 25, 15346−15352

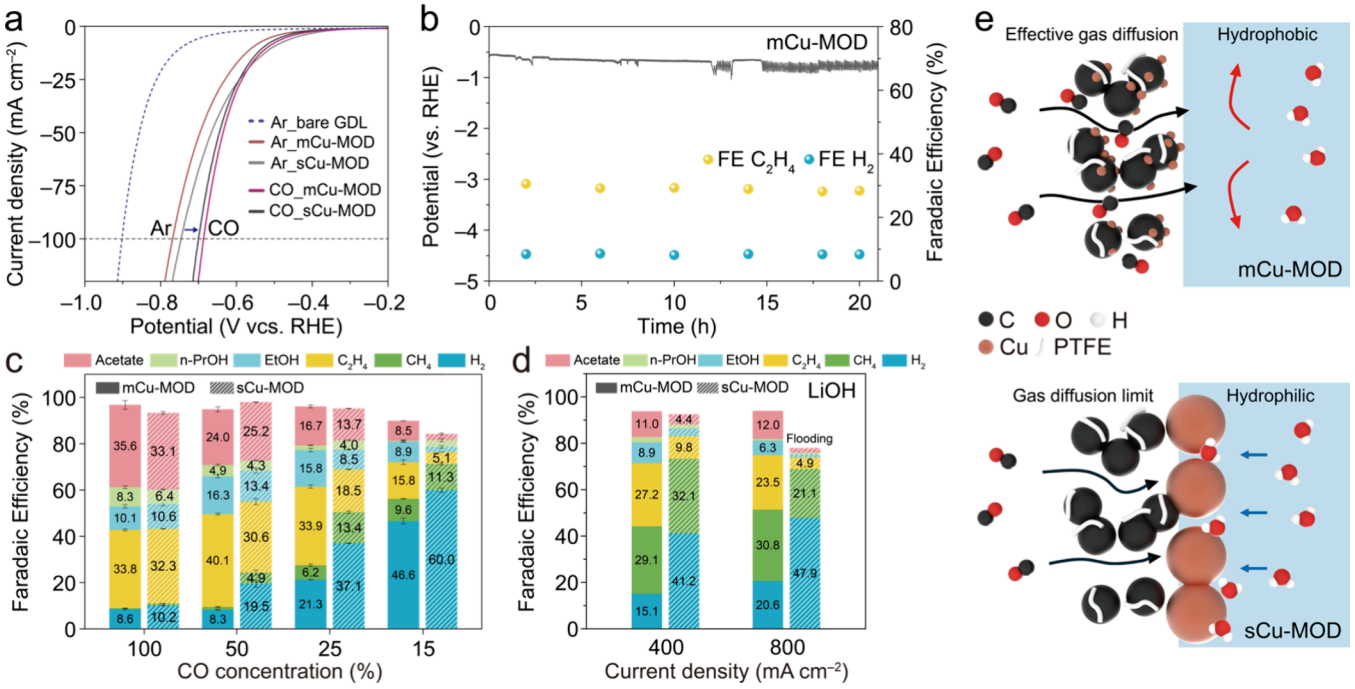

Figure 4. LSV curves of mCu-MOD and sCu-MOD GDEs under (a) Ar and CO atmospheres, respectively, at a scan rate of 10 mV s^{-1}. (b) Faradaic efficiencies for C_2H_4 and H_2 and cathodic potential of mCu-MOD at a current density of −400 mA cm^{-2} during the CORR. (c) Product distributions of the CORR on mCu-MOD and sCu-MOD GDEs in the flow-cell system at a current density of −400 mA cm^{-2} under various diluted CO (CO + N_2 mixture) conditions. (d) Product distributions of CORR on mCu-MOD and (b) sCu-MOD GDEs at current densities of −400 and −800 mA cm^{-2} in 1.0 M LiOH electrolyte measured in the flow-cell system. (e) Schematic of the surface wettability and CO diffusion of mCu-MOD and sCu-MOD GDEs during the CORR.

of electrolyte crossover during operation (Supporting Movies S1 and S2). Significant flooding of the sCu-MOD electrode occurred at 360 s, at which point the electrolyte passed through the MPL (liquid phase) to the MPS (gas phase), whereas mCu-MOD prevented water crossover (Figures 3b and S11). After the CORR, the CA of mCu-MOD was well preserved at 128.9°, whereas that of sCu-MOD decreased but remained high at 105.5° (Figure 3c).

Gaseous CO can be trapped within the GDE structure, enabling gas-phase diffusion rather than liquid-phase transport. This significantly shortens the diffusion path and enhances the local CO concentration, thereby improving mass transport and reaction kinetics.[13] The gas-phase product bubbles can be efficiently released through the hydrophobic capillaries, allowing the catalytically active sites to be maintained.[27−30] In contrast, sCu-MOD relies on a liquid-phase transport over a thin layer of surface Cu. Although both sCu-MOD and mCu-MOD may undergo Cu reconstruction via the formation of *CO−Cu complexes, the impact on the surface wettability is smaller when small NPs are placed within MPL.[31,32] The SEM and corresponding EDS images of mCu-MOD revealed modest Cu redeposition at high currents (Figure S12). Furthermore, the cross-sectional SEM-EDS image of the post-CORR mCu-MOD preserves its structural integrity after the reaction (Figure S13). In contrast, the thin film of sCu-MOD underwent substantial Cu particle loss and surface reconstruction. This suggests that once the electrolyte penetrates the newly exposed carbon surface of sCu-MOD, it may induce rapid GDE flooding.

Furthermore, to investigate the water fraction within the MOD electrodes under gas-feeding conditions, microscale in situ computed tomography (CT) analysis was carried out using a GDE-based membrane-electrode-assembly electrolyzer (MEA),[33,34] and CO_2 gas was fed to the cathode side for the CO_2RR. The 3D micro-CT images of the mCu-MOD electrode reveal the formation of small water droplets at a current density of −200 mA cm^{-2}, and the water droplet area increased at −400 mA cm^{-2} (Figure 3d). Further, the sCu-spt0.3 electrode exhibited significant wetting at −400 mA cm^{-2}, as shown by the higher water volume fraction based on the GDE volume (45.4% compared to 2.15% for mCu-MOD). (Figures 3e and S14). These results highlight the crucial role of the Cu infiltration method within the MPL in suppressing water fraction, even at high current densities. Therefore, the finely dispersed Cu NPs incorporated into the hydrophobic MPL preserve their porous structure, allowing for gas pathways and chemical accessibility. This facilitates efficient local CO diffusion and supports a balanced gas−liquid−solid interface.

To estimate the effect of gas diffusion on the reaction kinetics, linear sweep voltammetry (LSV) curves of sCu- and mCu-MOD obtained in the flow electrolyzer under Ar and CO were compared, revealing opposing activity trends.[9] Under an Ar atmosphere, sCu-MOD reached −100 mA cm^{-2} at a lower potential (−0.74 V) compared to that of mCu-MOD (Figure 4a), indicating the surface-exposed Cu on sCu-MOD can achieve fast HER kinetics from water dissociation. In comparison, under a CO atmosphere, mCu-MOD showed faster catalytic kinetics than sCu-MOD, suggesting higher CO gas accessibility to the active sites of the Cu NP positioned in the MPL. The differences in the CO mass-transport kinetics between the Cu-MOD GDEs became more pronounced at higher current densities (Figure S15). The current density of mCu-MOD reached −1200 mA cm^{-2} without fluctuation, whereas that of sCu-MOD showed clear signs of mass-

https://doi.org/10.1021/acs.nanolett.5c04051
Nano Lett. 2025, 25, 15346−15352

transport limitations over −600 mA cm^{-2}. The mCu-MOD electrode demonstrated high durability at a high current density of −400 mA cm^{-2} without any additives (e.g., PTFE), achieving only a 0.1% H_2 FE increase during 20 h of continuous reaction (Figure 4b). The high stability of the mCu-MOD can be attributed to the preservation of gas-accessible pathways and the mitigation of electrolyte flooding, and the structural advantage enables sustained CO transport to the active sites, thereby minimizing the HER.

To evaluate the local CO accessibility further, CORR was performed using CO feeds diluted by N_2 (Figure 4c).[35] Interestingly, mCu-MOD maintained a C_{2+} FE of 85.4%, even at 50% dilution, for the CORR at a current density of −400 mA cm^{-2}, whereas sCu-MOD showed a rapid increase in H_2 FE from 10.2% to 19.5%. The results from the CORR with the diluted feed gas indicate that utilizing the MPL layer in mCu-MOD enhances CO transport to the active sites while restricting the HER.[31,32,35] In addition, to examine the C−C coupling of the Cu-MOD electrodes affected by the microenvironment, CORR experiments were performed in the presence of Li^+. Li^+ decreases C−C coupling because of the decreased CO coverage induced by strongly hydrated Li^+ ions (Figure 4d).[36,37] In 1.0 M LiOH electrolyte, sCu-MOD showed a large increase in the H_2 FE to 41.2%, whereas its C_{2+} FE was reduced by 4.3 times to 19.2% at a current density of −400 mA cm^{-2} compared to that in 1.0 M KOH electrolyte. In contrast, the mCu-MOD maintained a C_2H_4 FE of 49.6% and hindered HER in the lithium-based electrolyte. These results also suggest that mCu-MOD maintains a higher local CO concentration, facilitating C−C coupling.[38−40] The efficient CO diffusion and hydrophobic microenvironment might enhance CO transport and maintain a balanced three-phase interface in the catalyst layers (Figure 4e).[13,35]

Herein, we have demonstrated how active Cu NPs integrated into the entire MPL GDE promote high-current CORR operation in a flow electrolyzer by increasing local CO accessibility and preserving the hydrophobic porous surface compared to the surface-loaded Cu GDEs. We develop a Cu deposition method by doctor-blading process using the metal−organic decomposition ink that enables low-temperature pyrolysis of copper precursor solution within the MPL of the carbon paper. This catalyst-loading strategy maintains a microporous hydrophobic surface without any additives and shortens the CO diffusion path, accelerating mass transport and preventing water fraction at high current densities. It allows a significantly enhanced mass activity of Cu for CORR. This hydrophobic microenvironment facilitates the release of gas-phase products within the MPL, thereby preserving the exposure of the active catalytic sites during the CORR. The sustained C−C coupling performance at diluted CO feeding also supports the increased CO local accessibility. Overall, we have reported a valuable electrode fabrication strategy that tunes the catalyst location in a commercial GDE for a highly enhanced and stable CORR.

■ ASSOCIATED CONTENT

Supporting Information

The Supporting Information is available free of charge at https://pubs.acs.org/doi/10.1021/acs.nanolett.5c04051.

Movie: In situ monitoring of gas-diffusion region corresponding to Figure 2b (MP4)

Detailed experimental section, additional material characterization, electrochemical performance, Cu loading amounts calculation, and water volume fraction (PDF)

■ AUTHOR INFORMATION

Corresponding Author

Yun Jeong Hwang − *Department of Chemistry, Seoul National University, Seoul 08826, Republic of Korea;* orcid.org/0000-0002-0980-1758; Email: yjhwang1@snu.ac.kr

Authors

Juhyung Choi − *Department of Chemistry, Seoul National University, Seoul 08826, Republic of Korea;* orcid.org/0000-0003-0770-6113

Sejin Park − *Department of Chemistry, Seoul National University, Seoul 08826, Republic of Korea*

Dayeon Kim − *Department of Chemistry, Seoul National University, Seoul 08826, Republic of Korea*

Hyun Chul Kim − *Clean Energy Research Center, Korea Institute of Science and Technology, Seoul 02792, Republic of Korea*

Hyewon Yun − *Department of Chemistry, Seoul National University, Seoul 08826, Republic of Korea*

Yewon Hong − *Department of Chemistry, Seoul National University, Seoul 08826, Republic of Korea*

Hyun Ji An − *Department of Chemistry, Seoul National University, Seoul 08826, Republic of Korea*

Taemin Lee − *Department of Energy Science and Engineering, Daegu Gyeongbuk Institute of Science and Technology (DGIST), Daegu 42988, Republic of Korea*

Noho Lee − *Air Science Research Center, Samsung Advanced Institute of Technology, Suwon 16678, Republic of Korea*

Jaeeun Kim − *Air Science Research Center, Samsung Advanced Institute of Technology, Suwon 16678, Republic of Korea*

Dae-Hyun Nam − *Department of Materials Science and Engineering, Korea University, Seoul 02841, Republic of Korea;* orcid.org/0000-0002-0871-1355

Hyung-Suk Oh − *Clean Energy Research Center, Korea Institute of Science and Technology, Seoul 02792, Republic of Korea; School of Advanced Materials Science & Engineering and KIST-SKKU Carbon-Neutral Research Center, Sungkyunkwan University (SKKU), Suwon 16419, Republic of Korea;* orcid.org/0000-0002-0310-6666

Complete contact information is available at: https://pubs.acs.org/10.1021/acs.nanolett.5c04051

Author Contributions

#J.C. and S.P. contributed equally to this work.

Notes

The authors declare no competing financial interest.

■ ACKNOWLEDGMENTS

This work was supported by Samsung Advanced Institute of Technology, Samsung Electronics Co., Ltd, and the National Research Foundation of Korea (NRF) grant funded by the Korean government (RS-2025-00515642), and partially supported by the Korea Evaluation Institute of Industrial Technology (Alchemist Project, NTIS- 2410013669, 20018904) through the Ministry of Trade, Industry and Energy, Korea. The authors also acknowledge the support of

the Global-LAMP program funded by the Ministry of Education, Korean government (No. RS-2023-00301976), and the Creative-Pioneering Researchers Program through Seoul National University.

REFERENCES

(1) Kim, J. Y. T.; Sellers, C.; Hao, S.; Senftle, T. P.; Wang, H. Different distributions of multi-carbon products in CO2 and CO electroreduction under practical reaction conditions. *Nat. Catal.* **2023**, *6* (12), 1115−1124.
(2) Alkayyali, T.; Zargartalebi, M.; Ozden, A.; Arabyarmohammadi, F.; Dorakhan, R.; Edwards, J. P.; Li, F.; Shayesteh Zeraati, A.; Fan, M.; Bazylak, A.; et al. Pathways to reduce the energy cost of carbon monoxide electroreduction to ethylene. *Joule* **2024**, *8* (5), 1478−1500.
(3) Guo, S.; Liu, Y.; Huang, Y.; Wang, H.; Murphy, E.; Delafontaine, L.; Chen, J. L.; Zenyuk, I. V.; Atanassov, P. Promoting Electrolysis of Carbon Monoxide toward Acetate and 1-Propanol in Flow Electrolyzer. *ACS Energy Lett.* **2023**, *8* (2), 935−942.
(4) Park, S.; Grigioni, I.; Alkayyali, T.; Lee, B.-H.; Kim, J.; Shirzadi, E.; Dorakhan, R.; Lee, G.; Abed, J.; Bossola, F.; et al. High carbon efficiency in CO-to-alcohol electroreduction using a CO reservoir. *Joule* **2023**, *7* (10), 2335−2348.
(5) Ding, J.; Li, F.; Ren, X.; Liu, Y.; Li, Y.; Shen, Z.; Wang, T.; Wang, W.; Wang, Y. G.; Cui, Y.; et al. Molecular tuning boosts asymmetric C-C coupling for CO conversion to acetate. *Nat. Commun.* **2024**, *15* (1), 3641.
(6) Ruqia, B.; Tomboc, G. M.; Kwon, T.; Kundu, J.; Kim, J. Y.; Lee, K.; Choi, S.-I. Recent advances in the electrochemical CO reduction reaction towards highly selective formation of Cx products (X = 1−3). *Chem. Catal.* **2022**, *2* (8), 1961−1988.
(7) Haaring, R.; Kang, P. W.; Guo, Z.; Lee, J. W.; Lee, H. Developing Catalysts Integrated in Gas-Diffusion Electrodes for CO(2) Electrolyzers. *Acc. Chem. Res.* **2023**, *56* (19), 2595−2605.
(8) Nguyen, T. N.; Dinh, C. T. Gas diffusion electrode design for electrochemical carbon dioxide reduction. *Chem. Soc. Rev.* **2020**, *49* (21), 7488−7504.
(9) Yang, K.; Kas, R.; Smith, W. A.; Burdyny, T. Role of the Carbon-Based Gas Diffusion Layer on Flooding in a Gas Diffusion Electrode Cell for Electrochemical CO2 Reduction. *ACS Energy Lett.* **2021**, *6* (1), 33−40.
(10) Burchardt, T. An evaluation of electrocatalytic activity and stability for air electrodes. *J. Power Sources* **2004**, *135* (1−2), 192−197.
(11) Popovic, S.; Smiljanic, M.; Jovanovic, P.; Vavra, J.; Buonsanti, R.; Hodnik, N. Stability and Degradation Mechanisms of Copper-Based Catalysts for Electrochemical CO(2) Reduction. *Angew. Chem., Int. Ed.* **2020**, *59* (35), 14736−14746.
(12) Wu, Y.; Charlesworth, L.; Maglaya, I.; Idros, M. N.; Li, M.; Burdyny, T.; Wang, G.; Rufford, T. E. Mitigating Electrolyte Flooding for Electrochemical CO2 Reduction via Infiltration of Hydrophobic Particles in a Gas Diffusion Layer. *ACS Energy Lett.* **2022**, *7* (9), 2884−2892.
(13) Xing, Z.; Hu, L.; Ripatti, D. S.; Hu, X.; Feng, X. Enhancing carbon dioxide gas-diffusion electrolysis by creating a hydrophobic catalyst microenvironment. *Nat. Commun.* **2021**, *12* (1), 136.
(14) Rabiee, H.; Ge, L.; Zhang, X.; Hu, S.; Li, M.; Yuan, Z. Gas diffusion electrodes (GDEs) for electrochemical reduction of carbon dioxide, carbon monoxide, and dinitrogen to value-added products: a review. *Energy Environ. Sci.* **2021**, *14* (4), 1959−2008.
(15) Chen, S.; Rowley, B.; Ganganahalli, R.; Yeo, B. S. Electroreduction of CO to 2.8 A cm(−)(2) C(2+) Products: Maximizing Efficiency with Minimalist Electrode Design Featuring a Mesopore-Rich Hydrophobic Copper Catalyst Layer. *Adv. Sci.* **2024**, *11*, No. e2405938.
(16) Li, M.; Idros, M. N.; Wu, Y.; Burdyny, T.; Garg, S.; Zhao, X. S.; Wang, G.; Rufford, T. E. The role of electrode wettability in electrochemical reduction of carbon dioxide. *J. Mater. Chem. A* **2021**, *9* (35), 19369−19409.
(17) Li, K.; Zou, S.; Zhang, J.; Huang, Y.; He, L.; Feng, X. Superhydrophobicity-Enabled Efficient Electrocatalytic CO2 Reduction at a High Temperature. *ACS Catal.* **2023**, *13* (14), 9346−9351.
(18) Tan, Y. C.; Lee, K. B.; Song, H.; Oh, J. Modulating Local CO2 Concentration as a General Strategy for Enhancing CC Coupling in CO2 Electroreduction. *Joule* **2020**, *4* (5), 1104−1120.
(19) Choi, Y.; Seong, K. d.; Piao, Y. Metal-Organic Decomposition Ink for Printed Electronics. *Adv. Mater. Interfaces* **2019**, *6* (20), DOI: 10.1002/admi.201901002.
(20) Shin, D. H.; Woo, S.; Yem, H.; Cha, M.; Cho, S.; Kang, M.; Jeong, S.; Kim, Y.; Kang, K.; Piao, Y. A self-reducible and alcohol-soluble copper-based metal-organic decomposition ink for printed electronics. *ACS Appl. Mater. Interfaces* **2014**, *6* (5), 3312−3319.
(21) Deore, B.; Paquet, C.; Kell, A. J.; Lacelle, T.; Liu, X.; Mozenson, O.; Lopinski, G.; Brzezina, G.; Guo, C.; Lafreniere, S.; et al. Formulation of Screen-Printable Cu Molecular Ink for Conductive/Flexible/Solderable Cu Traces. *ACS Appl. Mater. Interfaces* **2019**, *11* (42), 38880−38894.
(22) Sheng, A.; Islam, A.; Khuje, S.; Yu, J.; Tsang, H.; Bujanda, A.; Ren, S. Molecular copper decomposition ink for printable electronics. *Chem. Commun.* **2022**, *58* (68), 9484−9487.
(23) Chae, Y.; Kim, K.; Yun, H.; Kim, D.; Jung, W.; Hwang, Y. J.; Lee, U.; Lee, D. K.; Min, B. K.; Choi, W.; et al. Tailoring electrochemical CO2 reduction via substrate-induced gas diffusion. *J. Mater. Chem. A* **2023**, *11* (13), 7025−7033.
(24) Yang, Y.; Louisia, S.; Yu, S.; Jin, J.; Roh, I.; Chen, C.; Fonseca Guzman, M. V.; Feijoo, J.; Chen, P. C.; Wang, H.; et al. Operando studies reveal active Cu nanograins for CO(2) electroreduction. *Nature* **2023**, *614* (7947), 262−269.
(25) Wakerley, D.; Lamaison, S.; Ozanam, F.; Menguy, N.; Mercier, D.; Marcus, P.; Fontecave, M.; Mougel, V. Bio-inspired hydrophobicity promotes CO(2) reduction on a Cu surface. *Nat. Mater.* **2019**, *18* (11), 1222−1227.
(26) Niu, Z. Z.; Gao, F. Y.; Zhang, X. L.; Yang, P. P.; Liu, R.; Chi, L. P.; Wu, Z. Z.; Qin, S.; Yu, X.; Gao, M. R. Hierarchical Copper with Inherent Hydrophobicity Mitigates Electrode Flooding for High-Rate CO(2) Electroreduction to Multicarbon Products. *J. Am. Chem. Soc.* **2021**, *143* (21), 8011−8021.
(27) Kadyk, T.; Bruce, D.; Eikerling, M. How to Enhance Gas Removal from Porous Electrodes? *Sci. Rep.* **2016**, *6*, 38780.
(28) Bashkatov, A.; Park, S.; Demirkir, C.; Wood, J. A.; Koper, M. T. M.; Lohse, D.; Krug, D. Performance Enhancement of Electrocatalytic Hydrogen Evolution through Coalescence-Induced Bubble Dynamics. *J. Am. Chem. Soc.* **2024**, *146* (14), 10177−10186.
(29) Winther-Jensen, O.; Chatjaroenporn, K.; Winther-Jensen, B.; MacFarlane, D. R. Towards hydrogen production using a breathable electrode structure to directly separate gases in the water splitting reaction. *Int. J. Hydrog. Energy* **2012**, *37* (10), 8185−8189.
(30) Tiwari, P.; Tsekouras, G.; Wagner, K.; Swiegers, G. F.; Wallace, G. G. A new class of bubble-free water electrolyzer that is intrinsically highly efficient. *Int. J. Hydrog. Energy* **2019**, *44* (42), 23568−23579.
(31) Vavra, J.; Ramona, G. P. L.; Dattila, F.; Kormányos, A.; Priamushko, T.; Albertini, P. P.; Loiudice, A.; Cherevko, S.; Lopéz, N.; Buonsanti, R. Solution-based Cu+ transient species mediate the reconstruction of copper electrocatalysts for CO2 reduction. *Nat. Catal.* **2024**, *7* (1), 89−97.
(32) Yan, K.; Lee, S. W.; Yap, K. M. K.; Mule, A. S.; Hannagan, R. T.; Matthews, J. E.; Kamat, G. A.; Lee, D. U.; Stevens, M. B.; Nielander, A. C.; et al. On-line Inductively Coupled Plasma Mass Spectrometry Reveals Material Degradation Dynamics of Au and Cu Catalysts during Electrochemical CO(2) Reduction. *J. Am. Chem. Soc.* **2025**, *147* (5), 4079−4088.
(33) Park, J.; Kim, E.-D.; Kim, S.; Lim, C.; Kim, H.; Ko, Y.-J.; Choi, J.-Y.; Oh, H.-S.; Lee, W. H. Deriving an Efficient and Stable Microenvironment for a CO2MEA Electrolyzer by Reverse Osmosis. *ACS Energy Lett.* **2024**, *9* (7), 3342−3350.

(34) Ko, Y. J.; Lim, C.; Jin, J.; Kim, M. G.; Lee, J. Y.; Seong, T. Y.; Lee, K. Y.; Min, B. K.; Choi, J. Y.; Noh, T.; et al. Extrinsic hydrophobicity-controlled silver nanoparticles as efficient and stable catalysts for CO(2) electrolysis. *Nat. Commun.* **2024**, *15* (1), 3356.
(35) Sun, M.; Cheng, J.; Yamauchi, M. Gas diffusion enhanced electrode with ultrathin superhydrophobic macropore structure for acidic CO(2) electroreduction. *Nat. Commun.* **2024**, *15* (1), 491.
(36) Yan, W.; Wu, T.; Liu, J.; Zheng, Z.; Ma, M. Mass Transport-Dependent C-C Bond Formation for CO Electroreduction with Alkali Cations. *J. Am. Chem. Soc.* **2025**, *147* (11), 9990−10001.
(37) Malkani, A. S.; Li, J.; Oliveira, N. J.; He, M.; Chang, X.; Xu, B.; Lu, Q. Understanding the electric and nonelectric field components of the cation effect on the electrochemical CO reduction reaction. *Sci. Adv.* **2020**, *6* (45), No. eabd2569.
(38) Zhan, C.; Dattila, F.; Rettenmaier, C.; Bergmann, A.; Kuhl, S.; Garcia-Muelas, R.; Lopez, N.; Cuenya, B. R. Revealing the CO Coverage-Driven C-C Coupling Mechanism for Electrochemical CO(2) Reduction on Cu(2)O Nanocubes via Operando Raman Spectroscopy. *ACS Catal.* **2021**, *11* (13), 7694−7701.
(39) Deng, W.; Zhang, P.; Qiao, Y.; Kastlunger, G.; Govindarajan, N.; Xu, A.; Chorkendorff, I.; Seger, B.; Gong, J. Unraveling the rate-determining step of C(2+) products during electrochemical CO reduction. *Nat. Commun.* **2024**, *15* (1), 892.
(40) Song, J.; Zhang, H.; Sun, R.; Liu, P.; Ma, X.; Chen, C.; Guo, W.; Zheng, X.; Zhou, H.; Gao, Y.; et al. Local CO Generator Enabled by a CO-Producing Core for Kinetically Enhancing Electrochemical CO(2) Reduction to Multicarbon Products. *ACS Nano* **2024**, *18* (17), 11416−11424.

https://doi.org/10.1021/acs.nanolett.5c04051
Nano Lett. 2025, 25, 15346−15352